Solvent effects during the flash freezing fabrication of mesoporous polystyrenes

Sadaki Samitsu[1*], *Sirawit Pruksawan*[1,3,†], *Hideaki Yokoyama*[2], *Izumi Ichinose*[1]

[1] National Institute for Materials Science (NIMS), 1-2-1, Sengen, Tsukuba, Ibaraki 305-0047, Japan

[2] Department of Advanced Materials Science, Graduate School of Frontier Sciences, The University of Tokyo, 5-1-5 Toudaikasiwakyanpasu, Kashiwanoha, Kashiwa-shi, Chiba 277-8561, Japan

[3] Program in Materials Science and Engineering, Graduate School of Pure and Applied Sciences, University of Tsukuba, 1-1-1, Tenodai, Tsukuba, Ibaraki 305-8571, Japan

For Table of Contents use only

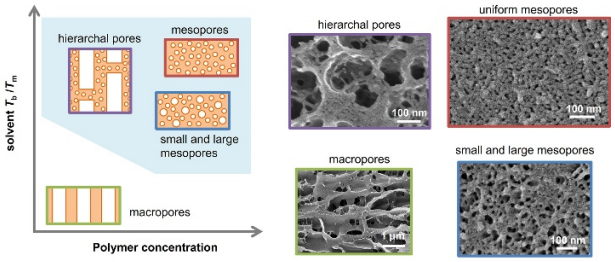

ABSTRACT

A polymer solution can be flash frozen to prepare homopolymers with mesoporous structures in a template-free manner. The flash freezing method is derived from the ice-templating or freeze-casting method. Herein, we comprehensively investigated the effects of 13 good solvents for polystyrene as well as the polystyrene concentration on the fabrication process. Solvents with high boiling-point-to-melting-point ratios yielded uniformly sized mesoporous polystyrenes at polymer concentrations ≥20 wt%. Such solvents provided a high specific surface area (328 m^2/g) and large mesopore volume (1.78 g/cm^3) at the optimal polystyrene concentration. Solvents with medium-boiling-point-to-melting-point ratios formed bimodal mesopores, while a low polystyrene concentration gave hierarchical structures composed of mesopores and macropores. These results provide an understanding of the mechanism associated with the formation of mesopores and enable control over the desired mesopore morphology.

INTRODUCTION

Mesoporous polymers are in strong demand for energy, environmental, and biomedical applications;[1–6] therefore, these methods for their fabrication have been widely developed over the past few decades,[7–10] most of which rely on block copolymers.[11–13] In particular, self-assembled block copolymer nanostructures have been used as templates for well-ordered mesopores,[14–18] as summarized in an excellent review article.[19] The block copolymer approach has also recently been extended to the fabrication of hierarchal pore structures.[20–22] Despite the great successes of block copolymers, fabricating mesoporous structures of commercially available homopolymers is a desirable objective from an industrial perspective.

Polymer solution phase separation[23] has been used to industrially fabricate porous polymers because it is simple, template-free, versatile, and has a high production rate. Fabrication methods based on liquid-liquid phase separation are well-known and have been described in polymer physics[24] and membrane science textbooks.[25] Nonsolvent-induced phase separation forms asymmetric macroporous membranes bearing mesopores only on their surfaces.[26] The thermally induced phase separation method enables the construction of homogeneous porous structures that contain almost-spherical interconnected pores.[27] Despite popular usage, preparation method are limited because pores larger than a few micrometers are obtained in the bulk,[28] and specific surface areas are usually less than 30 m^2/g.[29]

Liquid-solid phase separation driven by crystallization in solution is another principle that can be used to fabricate porous polymers. While polymer crystallization has been comprehensively investigated[30] and used to form membranes,[31] the method based on the crystallization of solvent molecules, otherwise known as "ice templating"[32] or "freeze casting,"[33,34] has, to the best of our knowledge, not been investigated in detail in the polymer science field. Pure solvent crystals grow when a polymer solution is cooled to a temperature below the melting point of the solvent, with polymer molecules selectively expelled and concentrated between crystals. Such a phase-separated structure remains porous after freeze-drying, thereby replicating the shapes of the solvent crystals. In addition, rapid crystal growth along a temperature gradient results in the formation of anisotropic hierarchical macropores.[35,36] Despite its impressive porous morphology, the pores of such a structure tend to be more than several tens of micrometers in size, with relatively small specific surface areas.[37] Based on the ice templating mechanism, mesopores will form if the solvent crystals can be reduced to several tens of nanometers in size. Small crystals usually form at high nucleation densities and under slow crystal-growth conditions, which is

satisfied by crystallization at low temperature, in accordance with common crystallization theory.[38]

Based on the abovementioned concept, we previously introduced a new method for fabricating mesoporous polymers inspired by the ice templating method, which is referred to as the "flash freezing method."[39] The flash freezing of a polymer solution facilitates solvent molecule crystallization at low temperature, which results in the co-continuous microphase separation of solvent nanocrystals and nanofibrous polymer networks. Since the solvent nanocrystals act as a spontaneous mesoporous template, solvent extraction at low temperature results in a mesoporous polymer with a large specific surface area (>300 m^2/g) as well as a sharp pore-size distribution in the 5–20 nm range, which successfully extends mesoporous designs achievable by phase separation methods. This method is facile, robust, and applicable to a wide range of commercially available homopolymers, including engineering thermoplastics with high glass-transition temperatures (T_g) (polystyrene, polycarbonate, polyvinylchloride, polyacrylonitrile, polysulfone, polyethersulfone, and polyetherimide). In addition to molding thick sheets, such mesoporous polymers can be shaped into films by casting and into fibers and pellets by spinning. The flash freezing method is efficient, scalable, and suitable for industrial applications. Previously,[39,40] we fabricated mesoporous polymers by flash freezing and demonstrated their potential applications, although the effect of the process parameters on the mesoporous morphology was not fully revealed. Hence, herein we report our investigations into the effects of solvent and polymer concentration on the flash freezing method (Figure 1). In particular, the effect of the solvent on the ice templating method has, to the best of our knowledge, not previously been investigated in a systematic manner. Interestingly, we found that the mesoporous morphology of a porous polystyrene is crucially affected by the ability of the solvent to

crystallize, which is directly related to its boiling-point-to-melting point ratio (T_b/T_m). In this study, we investigated the effects of T_b/T_m and polymer concentration on the morphology of mesoporous polystyrene. Furthermore, to understand the mechanism associated with phase separation driven by solvent nanocrystallization, we examine the crystallization kinetics of polymer solutions, especially during flash freezing at low temperature.

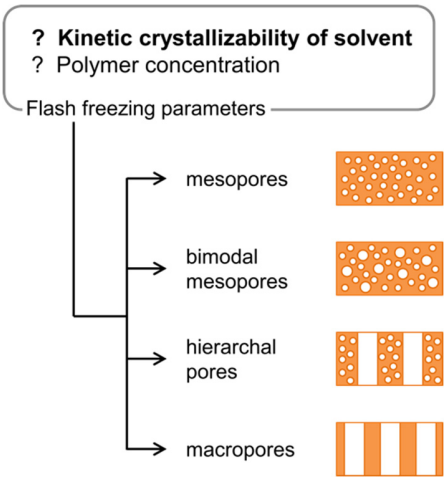

Figure 1. Parameters considered for the flash freezing method and the four types of pore morphology produced, including uniform mesopores, bimodal mesopores consisting of large and small mesopores, hierarchal pores containing macropores and mesopores, and macropores. While isolated mesopores are shown, they are interconnected in the three-dimensional bulk form.

EXPERIMENTAL

Flash freezing method

Reagent-grade organic solvents and commercial-grade polystyrene were purchased from Wako Chemicals, Japan, and were used as received. We selected polystyrene ($M_w \approx 200{,}000$) as a model polymer because it is highly soluble in a variety of organic solvents. Polystyrene solutions

were flash frozen using 13 good solvents for polystyrene with T_m values in the −70 to 15 °C range. The low-temperature limit was constrained to be the lowest temperature of the cryogenic refrigerator (VT-78HC, Nihon Freezer, Japan) used in this study. The T_m and T_b of each solvent were obtained from the literature[41,42] and are summarized in Table 1. The procedure used to fabricate porous polystyrene is shown in Scheme 1. Specifically, solid polystyrene was dissolved in the desired organic solvent with magnetic stirring at 25 ± 3 °C for 2–3 h or at 100 °C if not fully dissolved at room temperature. The polystyrene solution (10 g) was then added to a glass vial (diameter: 40 mm; height: 120 mm; glass-wall thickness: 1.3 mm) and quickly frozen onto the wall of the vial by horizontally rotating the vial in a liquid nitrogen bath (Scheme 1(b)). The thin (approximately 0.5–1.0-mm-thick) solution layer was frozen within 1 min, but was further cooled for an additional 5 min to ensure complete freezing. Excess pre-cooled methanol (−80 °C, 90 mL) was then added to the vial, which was maintained at −80 °C in a cryogenic refrigerator for 2–3 d. After warming to room temperature, the sample was further washed with methanol (twice, 50 mL) and solvent-exchanged with *tert*-butanol (twice, 50 mL). Mesoporous polystyrenes were subsequently obtained by freeze-drying the *tert*-butanol (usually for 1–2 days). Small pieces of solid porous polymers were usually collected because unintentional cracks appear in vitrified solutions during freezing process due to large thermal shrinkage. Hereafter, each porous polystyrene sample is referred to by the abbreviated solvent name and the polystyrene concentration; for example, “NB-40” refers to mesoporous polystyrene obtained from a 40 wt% nitrobenzene solution of polystyrene.

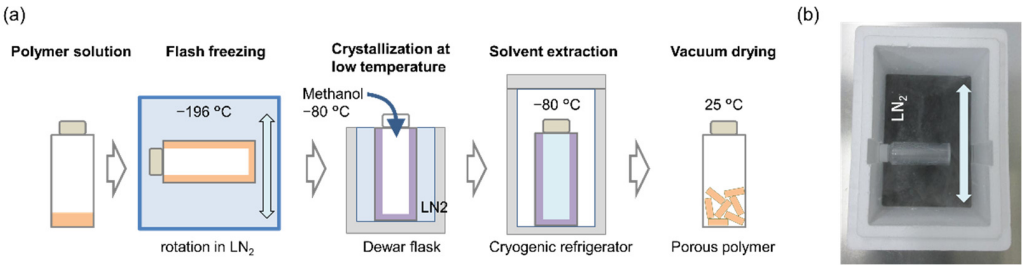

Scheme 1. (a) Outlining the flash freezing method. (b) Photographic image taken during flash freezing showing sample rolling in a liquid nitrogen (LN_2) bath.

Table 1. T_m and T_b values of organic solvents used in this study[41]

Solvent	Abbreviation	T_m (°C)	T_b (°C)	T_b/T_m[†]
1,4-Dioxane[‡]	Diox	−0.1[‡], 12.0	101.5	1.37
p-Xylene	pXy	13.4	138.5	1.44
1,2-Dichloroethane	DCE	−35.5	83.6	1.50
Carbon tetrachloride[‡]	CCl	−47.3[‡], −22.7	76.8	1.55
o-Xylene	oXy	−25.0	144.6	1.69
Nitrobenzene	NB	5.9	211.0	1.74
N,N-Dimethylacetamide	DMAc	−20.0	166.3	1.74
o-Dichlorobenzene	DCB	−16.9	180.6	1.77
Chlorobenzene	CB	−45.4	131.8	1.78
m-Xylene	mXy	−47.7	139.3	1.83
Cyclohexanone[‡]	cHxone	−52.2[‡], −31.9	155.8	1.94
N,*N*-Dimethylformamide	DMF	−60.3	153.2	2.00
1,1,2,2,-Tetrachloroethane[‡]	TCE	−65.7[‡], −43.6	145.3	2.02

[‡]Some of the solvents exhibit two T_m values due to the existence of polymorphs. The lower T_m corresponds to the transition from one crystal form to the other. Lower T_m values were obtained

from a database.[42] †T_b/T_m was calculated using units of absolute temperature (K). The lower T_m value was used for solvents with two T_m values.

Freezing and melting behavior of polystyrene solutions

The freezing and melting behavior of polystyrene solutions was monitored by differential scanning calorimetry (DSC; Q2000, TA instruments, USA), with the temperature controlled with a liquid nitrogen cooler. Characteristic behavioral temperatures, including crystallization temperature (T_f), cold-crystallization temperature (T_c), T_m, and T_g, were determined from the DSC curves. Enthalpy changes during phase transition, including crystallization enthalpy (ΔH_f), cold-crystallization enthalpy (ΔH_c), and melting enthalpy (ΔH_m), were determined by integrating DSC peaks. Procedural details are reported in our previous paper.[39]

Characterizing mesoporous polystyrenes

Porous polystyrenes were characterized by cross-sectional scanning electron microscopy (SEM; FE-SEM S-4800, Hitachi, Japan). The specific surface areas (S_{BET}) and meso, macro, and total pore volumes (V_{meso}, V_{macro}, and V_{total}) were evaluated through N_2 gas adsorption at −196 °C using a gas-adsorption analyzer (Belsorp-max, MicrotracBel, Japan). Procedural details are reported in our previous paper.[10,39]

Small-angle X-ray scattering (SAXS) experiments were performed on the BL-6A beamline at the Photon Factory of the High Energy Accelerator Research Organization (KEK) in Tsukuba, Japan. Further details regarding beamline setup are described elsewhere.[43] SAXS profiles were recorded at a scattering vector (q) in the 0.04–2.3 nm^{-1} range using an X-ray wavelength of 1.5 Å and a sample-detector distance of 2420 mm (calibrated using silver behenate). Each mesoporous polystyrene (approximately 0.5–1.0-mm-thick) was mounted onto a sample holder

and exposed to the X-ray beam for 1–10 s at room temperature. SAXS patterns were recorded using a photon-counting detector (PILATUS3 1M, DECTRIS, Switzerland). Each two-dimensional scattering image exhibited an isotropic pattern around the center of the beam and was converted into a one-dimensional scattering intensity profile by circular averaging. Data were processed using SAngler as described in the literature.[44] Peaks in the linear SAXS profiles were Gaussian curve fitted to provide characteristic wavenumbers (q_{SAXS}) that were converted into characteristic sizes (d_{SAXS}) using the equation: $d_{SAXS} = 2\pi/q_{SAXS}$.

RESULTS AND DISCUSSION

Crystallization behavior of nitrobenzene solutions and morphologies of the resulting porous polystyrenes

According to our previous study,[39] solvent molecule crystallization plays an important role during flash freezing. To confirm this, NB solutions with different weight percentages of polystyrene (C_{PS}) were subjected to DSC. The 20 wt% solution exhibited a large exothermic peak due to the crystallization of molecular NB, even upon flash freezing; this behavior is similar to that observed for the pure solvent (NB) (Figure 2(a)). Based on this peak, T_f was determined to be −26 °C, while ΔH_f is 51.0 J/g. The NB crystals melted at T_m = 4 °C during heating, as evidenced by an endothermic peak with ΔH_m = 60.1 J/g. In contrast, the 40 wt% solution only exhibited a baseline shift at T_g = −66 °C, consistent with a lack of crystallization; instead, the solution vitrified during flash freezing (Figure 2(b)). Subsequent heating revealed a broad exothermic peak at −44 °C that extended to 0.3 °C. In addition, peak integration yielded ΔH_c = 27.2 J/g, in agreement with the ΔH_m value of 28.0 J/g observed at T_m. The agreement between

ΔH_c and ΔH_m reveals that this exotherm is the result of the cold crystallization of molecular NB; importantly, this occurred at a (low) temperature close to T_g, which is 18 °C lower than T_f determined for the 20 wt% solution. The 40 wt% solution behaved in a similar manner to the 20 wt% DMF solution reported in our previous study.[39] Overall, the DSC traces show considerable differences in the crystallization behavior of NB solutions at C_{PS} = 20 and 40 wt%.

Porous polystyrenes were fabricated by flash freezing using 20 and 40 wt% solutions. As shown in Figure 2(c), the NB-20 porous polystyrene displays a framework with 100–200-nm-thick walls that formed anisotropic macropores, which are 0.5–1.0 μm wide and more than several micrometers long. The structure is dimensionally similar to those obtained by conventional ice templating[32] and corresponds to the macropores shown in Figure 1. In contrast, the low-magnification image of NB-40 shows no macropores, while a large number of mesopores are clearly evident in the high-magnification image (Figure 2(d)). In this case, the reticular structure of the 10–20-nm-thick nanofibers formed mesopores 10–15 nm in diameter that correspond to the uniform mesopores schematically depicted in Figure 1. These mesopores are ~100-times smaller than the macropores observed in the image of NB-20. Significantly, NB pore morphology and crystallization behavior are correlated, as confirmed by DSC.

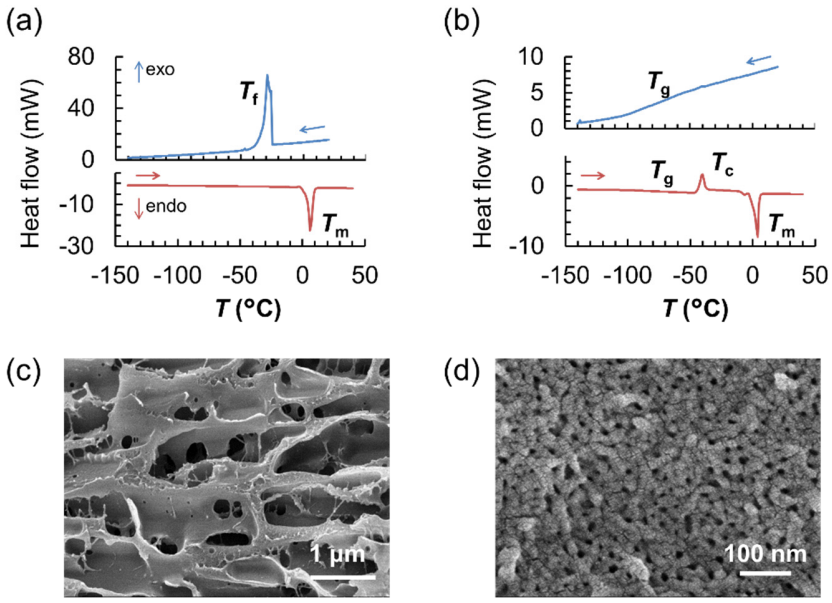

Figure 2. DSC curves of the NB solutions: (a) 20 wt% and (b) 40 wt% solutions. The solutions were flash frozen to −150 °C (upper panels) and subsequently heated to 40 °C at 10 °C/min (lower panels). Cross-sectional SEM images of the obtained porous polystyrenes: (c) NB-20, (d) NB-40.

The DSC data enabled the crystallization behavior of the NB solutions to be represented on a phase diagram (Figure 3(a)). As indicated, the T_m of the NB solution decreases slightly with increasing C_{PS}, a result of melting point depression in the polymer solution.[45] NB crystallized exothermically at low C_{PS} values (10–25 wt%), which enabled T_f to be determined. Since T_f exhibits a steeper C_{PS} dependence than T_m, the degree of supercooling ($\Delta T = T_m - T_f$) increases with C_{PS} to a value of 40 °C at C_{PS} = 25 wt%. Flash freezing resulted in polystyrene solution vitrification at $C_{PS} \geq 30$ wt%.

C_{PS} and T_g are related by the Gordon–Taylor expression (Eq. (1)):[46]

$$T_g = \frac{x_{PS}T_{gp} + k_{GT}(1-x_{PS})T_{gs}}{x_{PS} + k_{GT}(1-x_{PS})}, \quad (1)$$

where T_{gp} and T_{gs} are the T_g values of the polymer and the solvent, respectively, x_{ps} is the polymer volume ratio: $x_{ps} = (C_{PS}/\rho_p)/\{C_{PS}/\rho_p+(100 - C_{PS})/\rho_s\}$, ρ_p and ρ_s are the densities of the polymer and solvent, and k_{GT} is a specific parameter that expresses deviation from the simple additivity rule. The T_g values of the NB solutions were observed to decrease rapidly with decreasing C_{PS} owing to the low T_g of NB (i.e., −112 °C).[47] Eq. (1) was found to reasonably describe T_g behavior, which suggests that flash freezing provides a common glassy state for each polystyrene solution. Cold crystallization was observed close to the T_g curve when no considerable crystallization occurred during flash freezing; cold crystallization was then no longer observed at high C_{PS} values (> 60 wt%) because the T_m line is too close to the T_g curve, which prevents sufficient supercooling for cold crystallization.

Although the melting enthalpy measured for pure NB (ΔH_{m0} = 86.7 J/g) agrees with the database value,[42] the ΔH_f, ΔH_c, and ΔH_m values of the NB solutions depended significantly on C_{PS} (Figure 3(b)). Since ΔH_m was observed to decrease linearly with increasing C_{PS}, its relationship can be described by Eq. (2):

$$\Delta H_m = \Delta H_{m0}(1 - \alpha\, C_{PS}/100) \qquad (2)$$

, where Eq. (2) is defined at the C_{PS} range that gives $\Delta H_m \geq 0$.

Figure 3(b) shows that ΔH_m lies between 0 and ΔH_{m0}, while α, the slope of the linear plot, was calculated to be 1.62. The expected value of ΔH_m can be expressed as: $\Delta H_{m0} \times (1 - C_{PS}/100)$ when all NB molecules in solution crystallize. Hence, each value of ΔH_m determined by DSC was evidently smaller than the expected value because some NB molecules do not crystallize, as determined by α. The weight ratios of the total solvent, the uncrystallized solvent, and the crystallized solvent can be described by: $(1 - C_{PS}/100)$, $(\alpha - 1) \times C_{PS}/100$, and $(1 - \alpha C_{PS}/100)$, respectively.[45] Consequently, a C_{PS} of 61.7 wt% leads to $(1 - \alpha C_{PS}/100) = 0$ when α is 1.62,

revealing the presence of 38.3 wt% uncrystallized NB. In addition, polystyrene chains strongly bind to NB molecules and prevent their crystallization by slowing their molecular motions in the vicinity of the polymer chains when C_{PS} is >61.7 wt%. As a result, only the glassy solution state was observed at C_{PS} >61.7 wt%. In contrast, excess NB molecules that were not bound to polystyrene chains were able to crystallize during DSC at C_{PS} < 61.7 wt%. Nevertheless, polystyrene chains still affect the crystallization behavior of unbound NB molecules and alter their behavior even in this C_{PS} range, depending on the value of C_{PS}. Indeed, the plot shows two C_{PS} ranges in which ΔH_c is and is not observed; they are referred to as regions [1] and [3], respectively (Figure 3(b)). Region [1] corresponds to C_{PS} values in the 30–60 wt% range, which satisfies $\Delta H_c \approx \Delta H_m$ with a negligible value of ΔH_f. The majority of NB molecules do not crystallize during flash freezing in this region, but cold-crystallize instead during subsequent heating.

Flash freezing fabrication yield pore properties that depend on the abovementioned regions (i.e., regions [1] and [3]), as shown in Figure 3(c). More specifically, large S_{BET} values (≥165 m^2/g) and large V_{meso} values (≥0.40 g/cm^3) were observed for region [1], whereas low S_{BET} values (≤61 m^2/g) and negligible V_{meso} values were observed for region [3]. The large values of S_{BET} and V_{meso} observed in region [1] highlight the importance of $\Delta H_c \approx \Delta H_m$, conditions under which a considerable number of NB molecules crystallize at (low) temperatures close to T_g. The relationship between C_{PS} and ΔH_f and ΔH_c reveals that a high C_{PS} is desirable when fabricating a mesoporous polymer; the mechanism associated with this observation is further discussed below (*vide infra*). We note that porous polystyrene fabrication has an upper C_{PS} limit of 40 wt% because solvent exchange does not proceed efficiently at C_{PS} >40 wt%. Although a C_{PS} >40 wt%

enables solvent molecules to crystallize, the solvent crystals are likely to be isolated rather than interconnected, which hinders solvent exchange and an inability to fabricate a porous polymer.

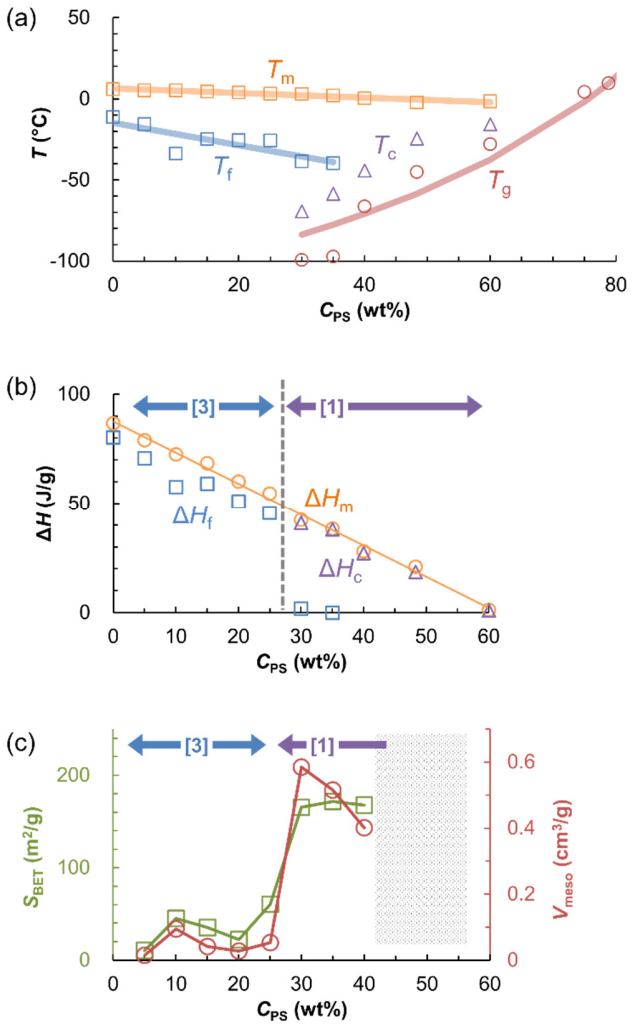

Figure 3. (a) Phase diagram of NB solutions from DSC data obtained during flash freezing and heating at 10 °C/min. The T_m and T_f depressions are linearly fitted: $T_m = 6.4 - 0.14 \times C_{PS}$ (orange line) and $T_f = -14.7 - 0.69 \times C_{PS}$ (blue line). The T_g curve shown in red is calculated using equation (1) with $T_{gp} = 100$ °C, $T_{gs} = -112$ °C, and $k = 3.19$. (b) Enthalpies of NB solutions at melting ΔH_m (circles), crystallization ΔH_f (squares), and cold crystallization ΔH_c (triangles) as functions of C_{PS}. ΔH_m values decrease linearly with increasing C_{PS}: $\Delta H_m = 86.7 \times (1 - 0.0162 \times C_{PS})$. The two regions in which ΔH_c values are and are not observed are referred to as [1] and [3].

(c) S_{BET} and V_{meso} values of porous polystyrene as a functions of C_{PS}. These values discretely increase as C_{PS} transitions from region [3] to region [1].

The effect of solvent type

As discussed above, the ability of the solvent to crystallize, which significantly influences the resulting porous structure, is a key parameter of the flash freezing method. Research into the glassy states of organic molecules revealed that the kinetic crystallizability (i.e., the opposite of the glass-forming ability) of a molecule is directly related to its T_b/T_m ratio, with a large T_b/T_m ratio resulting in low kinetic crystallizability.[48] Based on this correlation, we tested 13 good solvents for polystyrene with various T_b/T_m ratios by fabricating porous polystyrenes from 30 wt% solutions using the flash freezing method. The S_{BET} and V_{meso} values of the porous polystyrenes are plotted as functions of T_b/T_m in Figure 4(a), which reveals that the 10 solvents with $T_b/T_m \geq 1.50$ gave high S_{BET} values (120–298 m^2/g) and V_{meso} values of 0.46–1.32 cm^3/g. In addition, large numbers of mesopores were visually confirmed by SEM (Figures 4(b) and S1). These results show that various organic solvents can be used to prepare mesoporous polystyrenes, which validates the robustness of the developed method. The two solvents (Diox and pXy) with low T_b/T_m ratios (≤ 1.44) were confirmed to form only macropores without any mesopores, resulting in low S_{BET} and V_{meso} values (Figure S2(a)). Macropore formation correlates with the crystallization behavior of the solution in region [3] (Figure S2(b,c)), which is in agreement with observations made for the NB solutions. Figure 4 shows that the T_b/T_m ratio clearly divides the S_{BET} and V_{meso} trends, thereby providing a simple but informative parameter that distinguishes our method from those previously reported.[49,50] In cryogel freeze-drying, a solvent with a high T_m and a low T_b value (i.e., a low T_b/T_m ratio) that ensures a practical

sublimation rate is preferred. Water, with a low T_b/T_m of 1.37, is the most commonly used solvent for this method, with Diox and pXy used as alternative solvents for water-insoluble polymers.[51,52] Solvents with low T_b/T_m ratios are highly crystallizable and usually form only macropores while preventing the formation of mesopores. In contrast, our developed method uses solvents with large T_b/T_m ratios that facilitate the fabrication of mesoporous polymers through crystallization at low temperatures.

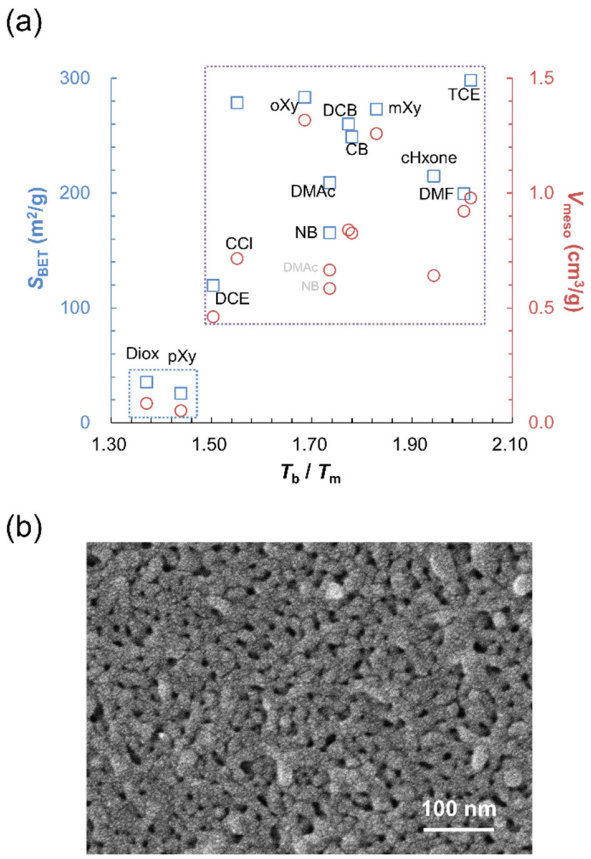

Figure 4. (a) S_{BET} and V_{meso} of porous polystyrene as functions of the T_b/T_m ratio of the solvent. The porous polystyrenes were fabricated from 30 wt% solutions by the flash freezing method using 13 different solvents. (b) Cross-sectional SEM image of the TCE-30 sample.

Effect of concentration on the mesoporous structure

DMF is a suitable solvent for fabricating mesopores because of its relatively high T_b/T_m ratio, as presented in Table 1. The phase diagram for DMF solutions (Figure 5(a)) shows that solutions with C_{PS} values in the 5–10 wt% range crystallize during heating and cooling; this region in the diagram is referred to as region [2]. In contrast, those with C_{PS} values in the 15–40 wt% range only undergo cold crystallization during heating, which corresponds to region [1]. Mesopores with large S_{BET} values (183–282 m^2/g) and V_{total} values of 0.94–2.39 cm^3/g are formed in both regions [1] and [2]. The 5–40 wt% C_{PS} range (Figure 5(b)) is significantly wider than that of region [1] observed for the NB solutions (30–40 wt% in Figure 3(c)). As discussed later (*vide infra*: Figure 11) a C_{PS} of 5–10 wt% (region [2]) provides macropores as well as mesopores that correspond to the hierarchal pores shown in Figure 1.

C_{PS} significantly influences mesoporous polymer pore size in an ordered manner in region [1] (C_{PS} of 15–40 wt%), as shown in Figure 5(c). These data are consistent with SEM observations. More specifically, a significantly larger pore volume was obtained at a pore diameter (d) of 60–200 nm for DMF-15, and the pore-diameter distribution peaked at d_{peak} = 98 nm. The distribution gradually moved to smaller values of d and V_{total} with increasing C_{PS}. In contrast, DMF-40 presented a sharp single peak at d_{peak} = 15 nm, with a large V_{meso} of 0.93 cm^3/g. This lower V_{total} is the result of a lower solvent fraction because the volume of crystallizable solvent roughly determines the upper V_{total} limit. In addition, d_{peak} was observed to monotonically decrease with increasing C_{PS} (Figure 5(d)). In a similar manner, Gutiérrez et al. investigated fabricating porous poly(vinyl alcohol)s using the ice templating method, in which aqueous solutions are frozen in liquid nitrogen, and found that average pore size decreased with increasing polymer concentration in the 2.5–10 wt% range.[37] They also reported that the average pore size decreased as the freezing rate and the average molecular weight of the poly(vinyl alcohol) increased.

Although the observed concentration dependence is consistent with that observed in the current study, the reported pores are micrometer in size; i.e., nearly two orders of magnitude larger than those obtained in this study, which is attributable to the fact that the previous study used water (with a low T_b/T_m of 1.37), which crystallizes rapidly, while our method uses a solvent with a $T_b/T_m \geq 1.55$ and a high polymer concentration, which prevents the formation of solvent macrocrystals and results in mesoporosity.

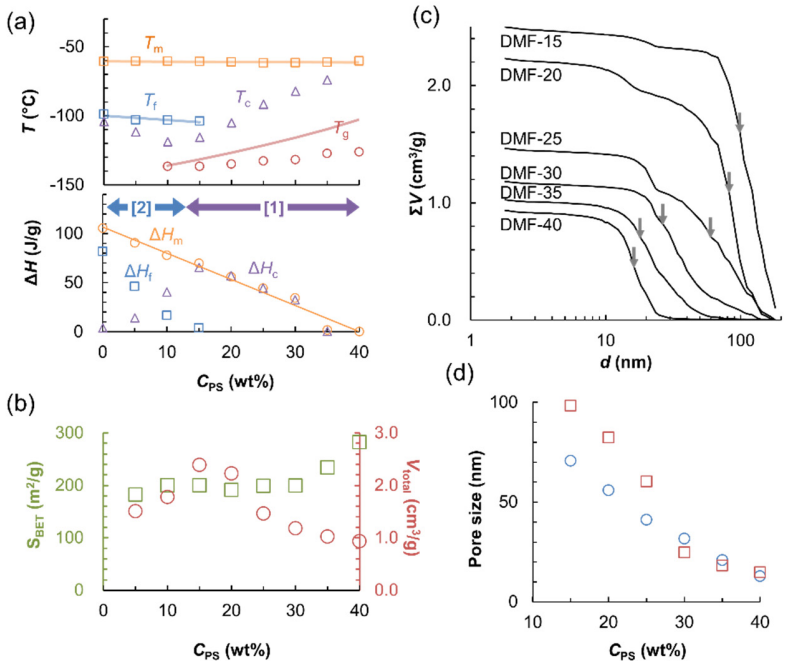

Figure 5. (a) (Upper) Phase diagram for DMF solutions determined from DSC curves recorded upon flash freezing and heating at 10 °C/min. The T_m and T_f depressions are linearly fitted: $T_m = -60–6 - 0.016 \times C_{PS}$ (orange line) and $T_f = -100–0 - 0.309 \times C_{PS}$ (blue line). The red T_g curve was calculated from equation (1) using $T_{gp} = 100$ °C, $T_{gs} = -144$ °C,[47] and $k = 2.98$. (Lower) Enthalpy changes of the DMF solutions as functions of C_{PS}. The ΔH_m values were observed to decrease linearly with increasing C_{PS}, with: $\Delta H_m = \Delta H_{m0} –1 - 0.0250 \times C_{PS}$). Regions [2] and [1] can be identified on the basis of the observed dependences of ΔH_f and ΔH_c, respectively. (b) S_{BET} and V_{total} values of the porous polystyrenes obtained from the DMF solutions as functions of C_{PS}.

(c) Cumulative pore volumes of mesoporous polystyrenes obtained from DMF solutions. (d) Pore size (squares) and d_{peak} (circles, determined from the pore-size distribution acquired by gas-adsorption measurements) as functions of C_{PS}. Pore sizes were calculated numerically according to a simple geometrical model (Figures S3 and S4, Supporting Information).

Crystallization kinetics at low temperature

With the aim of investigating crystallization behavior at low temperature, crystallization kinetics were examined by isothermal DSC using DMF solutions. No crystallization was observed when a 15 wt% solution was flash frozen, after which isothermal crystallization was observed at −96, −98, and −118 °C in the exotherms (Figure 6(a)). Crystallization was delayed for 19 min during isothermal crystallization at −96 °C, which is ascribable to low crystal-nucleation frequency; a sharp exothermic peak was observed beyond this timepoint due to rapid crystal growth. In contrast, crystallization was initiated within 2 min at −98 °C; hence, lower temperatures significantly accelerate the nucleation process. In fact, since crystallization starts immediately below 99°C, DSC could not monitor the induction time of less than 1 minute. A much broader exothermic peak was observed at −118 °C, consistent with slower DMF crystal growth at this temperature. Since nucleation and growth rate depend oppositely on temperature, the crystallization rate, which is the product of the nucleation and growth rates, is fastest at −104 °C for the 15 wt% solution, and decreases with decreasing or increasing temperature (Figure 7(a)). Upon crystallization at −104 °C, an exotherm appeared immediately, and a significantly broad exotherm was observed when C_{PS} increased from 15 to 25 wt%. The behavior is consistent with rapidly nucleating DMF crystals that grow extremely slowly (Figure 6(b)). This indicates that the nucleation rate is independent of $C_{PS;}$ however, growth rate depends significantly on C_{PS}. The high viscosities of the polymer solutions result in slow crystal growth at low crystallization

temperatures and/or high C_{PS}, which suppress the diffusive motions of solvent molecules. In addition, a high nucleation rate favorable for mesoporous polymer fabrication is achieved by crystallization at low temperature, which is almost unaffected by a high C_{PS} value.

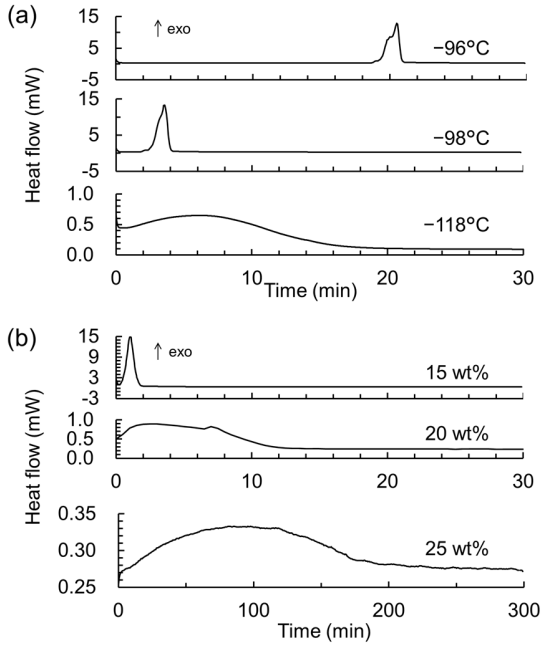

Figure 6. Isothermal crystallization behavior of the DMF solutions: (a) PS concentration of 15 wt%, and (b) crystallization temperature of −104 °C. The solutions were rapidly cooled from room temperature to the desired crystallization temperature, with heat flow recorded for the desired time.

The temperature- and C_{PS}-dependences of the crystallization kinetics are summarized in the form of a time–temperature–transformation (TTT) diagram, based on the isothermal crystallization data presented above (Figure 7(a)). The crystal region is drawn as a C-shaped curve in the diagram because higher temperatures delay crystal nucleation, while lower temperatures slow down crystal growth, with the highest crystallization rate corresponding to the “nose” of the

curve.[38,53] Although the induction time for crystallization is less than a few minutes at the "nose," and independent of C_{PS}, increasing the C_{PS} value significantly delays the crystallization-rate maximum. This delay is therefore ascribable to slower crystal growth due to the high viscosity of the solution. This delay also explains the dependence of C_{PS} on T_f and ΔT, consistent with the kinetics mechanism; hence, flash freezing results in preferential vitrification at high C_{PS}. This diagram also reveals that crystallization rarely occurs at crystallization temperatures above −91 °C owing to the negligible crystal-nucleation frequency. Interestingly, in contrast to the lack of crystallization observed under isothermal conditions (Figure 7(a)), cold crystallization occurred between −91 and −74 °C under temperature-scanning conditions (Figure 5(a)), probably because the temperature reduced to −140 °C, which promotes crystal nucleation. Crystal growth proceeds even at temperatures higher than the upper bound of the TTT diagram when crystal nuclei are present in solution. Our fabrication process freezes a polymer solution in liquid nitrogen, which possibly promotes the formation of crystal nuclei and assists in the formation of solvent nanocrystals.

As shown in Figure 7(b), the crystallization behavior of the solvent molecules is governed by the competition between their freezing and crystallization rates. The temperature cooling profile intersects with the upper part of the crystallization region at a low freezing rate, or low C_{PS}, or when the solvent is highly crystallizable, which determines the value of T_f (Figure 7(b), left). This process corresponds to the typical ice-templating or freeze-casting situation, which is referred to as "route A," as indicated in the phase diagram in Figure 8(a). Crystallization occurs at high T_f in this case, where low nucleation density and high growth rate form large solvent crystals that result in the generation of macropores upon solvent removal. In contrast, flash freezing vitrifies the solution and cold crystallization proceeds at low temperature when gently

heated in the opposite case, namely at a high freezing rate, high C_{PS}, and when solvent kinetic crystallizability is low (Figure 7(b), right). This process corresponds to our flash freezing method, which is referred to as "route B" in the phase diagram shown in Figure 8(a). This process satisfies the conditions of high nucleation density and low growth rate, and generates a large number of solvent nanocrystals that result in mesopore formation. In addition to freezing-rate control, the flash freezing method can be used to control the crystallization behavior of solvent molecules by optimizing the effects of polymer concentration and solvent kinetic crystallizability. It should be noted that the crystallization temperature used in the flash freezing fabrication method in this study was fixed at −80 °C due to the limitations of the experimental setup.

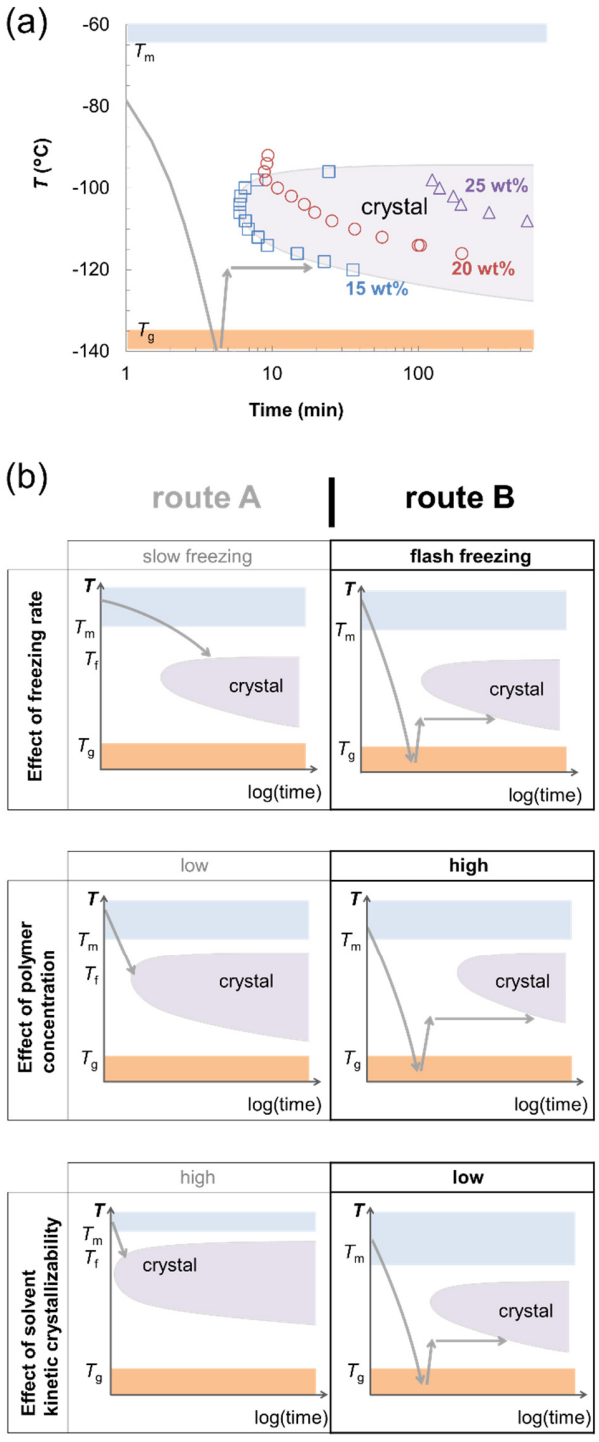

Figure 7. (a) Time–temperature–transformation (TTT) diagram for DMF solutions constructed from isothermal DSC data: C_{PS} = 15 wt% (squares), 20 wt% (circles), and 25 wt% (triangles). The crystallization time depicts the offset time of the exothermic peak, which represents almost

complete crystallization at that specific temperature. (b) Schematic illustration of the TTT diagram in terms of the effect of freezing rate (upper), C_{PS} (middle), and the kinetic crystallizability of the solvent (bottom). T_f appears at the intersection of the temperature cooling profile and the upper boundary of the C-shaped crystallization region in the left-hand panel.

Proposed mechanism for mesopore formation and pore-size control

We propose a mechanism that determines mesopore size based on the polymer solution phase diagram. The phase diagram in Figure 8(a) shows two crystallization pathways, as discussed in the previous section, namely route A, which takes place at low C_{PS} and/or with slow freezing and/or with a highly crystallizable solvent (i.e., the conventional method), and route B, which takes place at high C_{PS} and/or with flash freezing and/or with a poorly crystallizable solvent (i.e., the flash freezing method). In route A, solvent crystallization occurs unintentionally at T_f, which results in rapid crystal growth and the formation of macrocrystals. Explaining macropore size in a quantitative manner is difficult due to inhomogeneous nucleation, the directional growth of solvent crystals, and the undetermined crystallization temperature. In contrast, crystallization begins at a low temperature close to T_g in route B (point B1). A large number of solvent nuclei are generated at this temperature, and each nucleus grows particularly slowly, consistent with the assumption of homogeneous nucleation. Solvent crystals facilitate the participation of only solvent molecules in the crystal arrangement, excluding polymer molecules and preventing solvent crystal contamination. Owing to limited polymer diffusion at low temperature, spontaneous polymer discharge causes C_{PS} to increase locally around the crystal (Figure 8(b), left); this local C_{PS} increases with crystal grow (indicated by the arrow connecting B_1 to B_2 in the phase diagram), as shown by the horizontal arrow, which results in the formation of a

concentrated polymer phase around the crystal. The concentrated polymer phase vitrifies to form a glassy shell that surrounds the solvent crystal and restricts further crystal growth when the arrow meets the T_g line (point B_2) (Figure 8(b), right). According to the proposed mechanism, the uniform polymer solution results in co-continuous phase separation of the solvent crystals and the glassy polymer shell between the crystals; we assume local mass balance between the solvent crystals ($C_{PS} = 0$) and the glassy polymer shell (C_{PS} on the T_g curve) when this phase separation occurs locally, as indicated by the hatched regions in Figure 8(b). As a result, the difference in the C_{PS} of the initial solution and the C_{PS} on the T_g line at the crystallization temperature determines the crystal size. A high initial C_{PS} results in a small increase in the local C_{PS}, which causes the concentrated polymer phase to readily vitrify, thereby reducing solvent crystal size and generates small mesopores upon solvent removal. Based on the proposed mechanism, we considered a simple geometric model for the crystallization-driven phase separation process and quantitatively calculated pore size (see details in the Supporting Information, Figures S3 and S4). The d_{peak} values determined for the mesoporous polystyrenes obtained using DMF roughly agree with the pore sizes calculated by the model (Figure 5(d)).

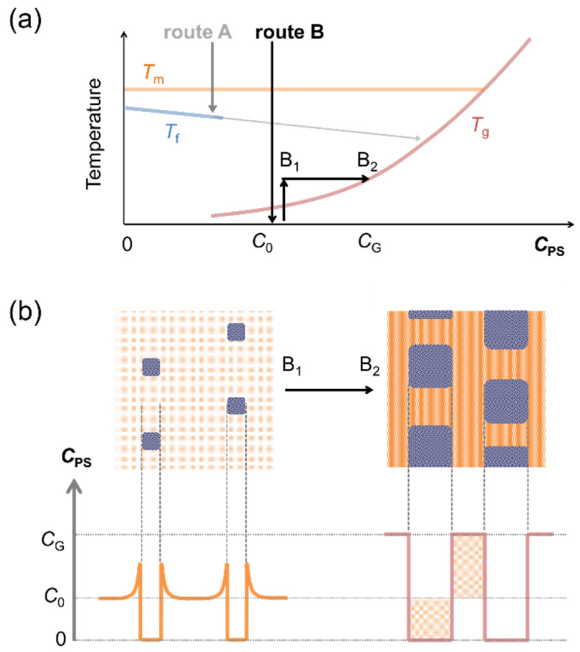

Figure 8. (a) Proposed crystallization pathways (route A and route B) schematically illustrated on the temperature–concentration phase diagram (Figure 7(b)). Route A represents the ice-templating method that typically relies on slow freezing at low C_{PS} (see Figure 2(a)), while route B represents our flash freezing method that relies on flash freezing at high C_{PS} (see Figure 2(b)). (b) Schematically illustrating the nanocrystallization process highlighted by the horizontal arrow (B_1 to B_2) in panel (a). A large number of crystal nuclei are simultaneously generated at low temperature (i.e., at point B_1) and grow slowly as the polymer concentrates around each crystal. The polymer concentration between crystals increases to that on the glass transition line (i.e., at point B_2) and crystal growth is prohibited by the formation of a glassy shell of the highly concentrated polymer solution. Due to the mass balance of the polymer, two hatched regions in the lower panel have the same area.

We fabricated 62 porous polystyrenes using 13 good solvents and a 5–40 wt% C_{PS} range to comprehensively demonstrate the influence of both C_{PS} and solvent on mesoporosity. The porous

structures were characterized by SEM and N_2-adsorption studies, the results of which are summarized in Table S1. In addition to uniform mesopores and macropores, we found additional unique morphologies, including hierarchal porous structures consisting of mesopores and macropores, and one with a bimodal mesopore distribution. The four types of porous structure are presented in terms of their S_{BET}-dependent V_{meso} and V_{total} values (Figure 9(a)). Despite slight data-point variations, V_{meso} was observed to generally increase with increasing S_{BET}. The largest V_{meso} value of 1.78 cm^3/g was found for oXy-30, and corresponds to an apparent porosity of 65%. In addition, the largest S_{BET} value of 328 m^2/g was recorded for mXy-20. The cross-sectional SEM images of oXy-30 and mXy-20 confirm the presence of numerous mesopores (Figure 9(b)). Furthermore, 14 macroporous polystyrenes are located in regions that correspond to small S_{BET} and V_{meso} values, and are clearly separated by other mesoporous polystyrenes. Because the three types of mesoporous polystyrene overlap in the $S_{BET} - V_{meso}$ plot, they were classified using additional morphological information based on SEM and pore-size data obtained from N_2-adsorption studies. Uniform mesopores are characterized by SAXS and mechanisms for the formation of the structures containing hierarchical pores and bimodal mesopores are discussed in the following sections.

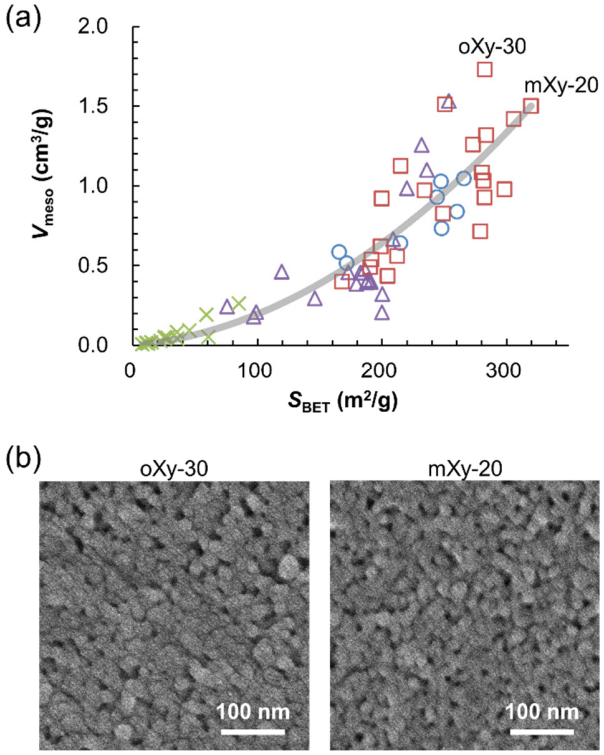

Figure 9. (a) Relationship between the S_{BET} and V_{meso} values of 62 porous polystyrenes prepared using 13 different solvents and C_{PS} = 5–40 wt%. The solid line represents the fitted curve: $V_{meso} = 1.24 \times 10^{-5} (S_{BET})^2 + 8.26 \times 10^{-4} (S_{BET})$. The four porous structures are represented by different symbols: squares = uniform mesopores, crosses = macropores, triangles = hierarchal pores, and circles = bimodal mesopores. (b) Cross-sectional SEM images of oXy-30 and mXy-20.

Confirming uniform mesopores by SAXS

Mesoporous polystyrenes with uniform pore-size distributions were prepared by selecting appropriate solvents and C_{PS} values. Their mesopore size distributions were analyzed by N_2-adsorption (Figure 10(a)), and the relationship between V_{meso} and d_{peak} is shown in Figure 10(b). The formation of uniform mesopores was confirmed by SEM (Figure S5), and the SAXS profile of each mesoporous polystyrene revealed a single peak that originates from its structural

periodicity (Figure 10(c)). The characteristic mesopore size of each polymer (d_{SAXS}) shows a close correlation with d_{peak} determined by gas adsorption (Figure 10(d)), which indicates that structural periodicity is related to mesopore size and confirms that uniformly sized pores are distributed throughout the bulk specimen.

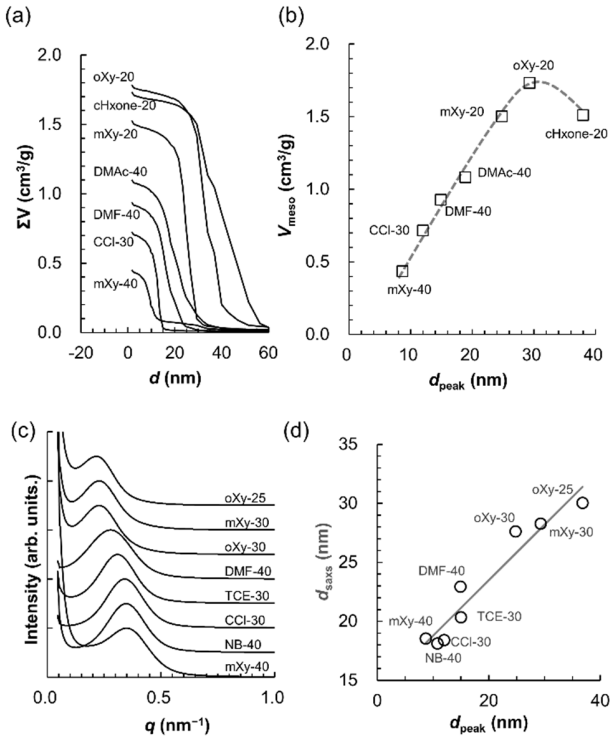

Figure 10. (a) Cumulative pore volumes of mesoporous polystyrenes with uniform mesopores. (b) V_{meso} as a function of d_{peak} for the mesoporous polystyrenes presented in (a). (c) SAXS profiles as functions of q. (d) Relationship between d_{SAXS} and d_{peak}. The solid line highlights the close correlation between d_{SAXS} and d_{peak}; i.e., $d_{SAXS} = 14.1 + 0.47 \times d_{peak}$.

Hierarchical pores

The porous polystyrene formed when the flash freezing method was applied to a low C_{PS} solution occasionally presented a hierarchical structure composed of both macropores and mesopores. The macropores are clearly observable by SEM, while the mesopores were detected

by N_2-adsorption studies (Figures 11(a) and 11(b)). For example, the SEM image of oXy-10 shows a lamellar-like morphology of thin sheets that formed slit-like macropores between sheets. cHxone-10 exhibited a sponge-like morphology with mesopores on the skeletons of the sponge; similar morphologies were also observed for oDCB-10 and CCl-10 (Figure S6). Solvents with moderate T_b/T_m ratios, such as DCE and DMAc, occasionally led to hierarchical pores at moderate C_{PS} values (Figure S7).

The process that forms hierarchal pores is shown schematically in Figure 11(c). Some solvent molecules crystallize as macrocrystals during flash freezing to low temperature; this partial crystallization was detected by DSC as a small exothermic peak upon flash freezing (Figure S8). Such crystal growth results in the retention of the remaining solvent molecules as a concentrated solution between the formed macrocrystals. Subsequent holding at a temperature near to but above T_g results in additional crystal nucleation of solvent in the concentrated solution and the formation of solvent nanocrystals between the macrocrystals. After extracting the solvent macro- and nanocrystals with cold methanol, the macropores were formed on mesoporous framework, resulting in the formation of hierarchal pores.

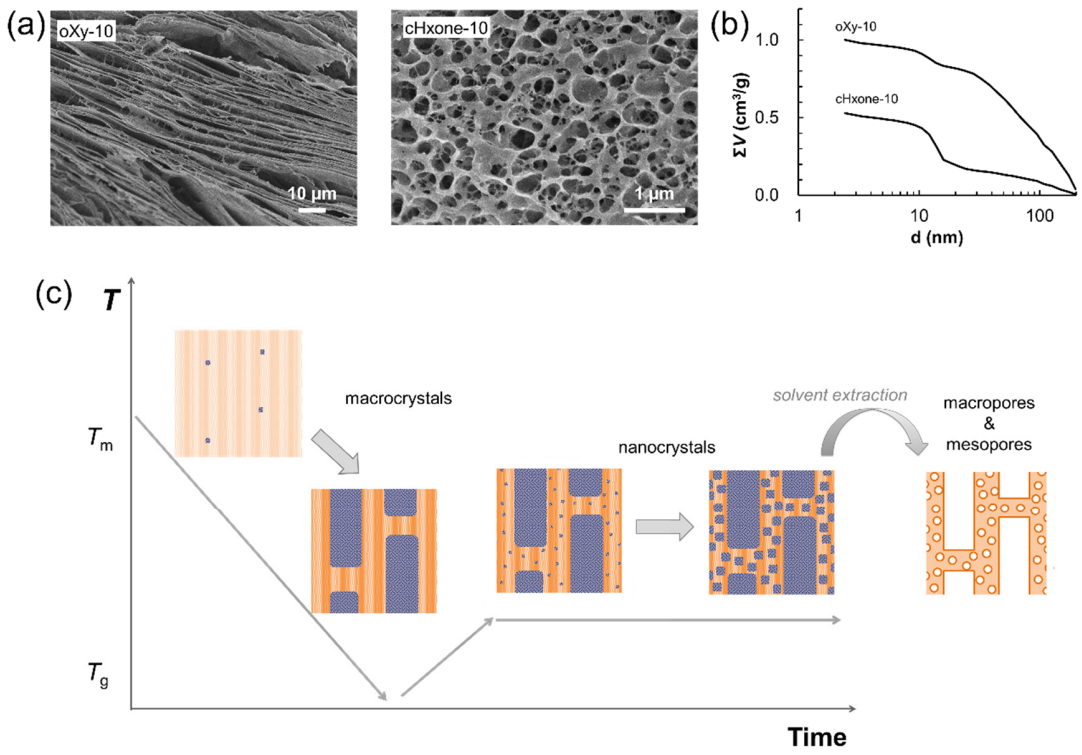

Figure 11. (a) Cross-sectional SEM images and (b) pore-size distributions of porous polystyrenes with hierarchical porous structures composed of mesopores and macropores. oXy-10: S_{BET} = 179 m^2/g, V_{meso} = 0.39 cm^3/g. cHxone-10: S_{BET} = 191 m^2/g, V_{meso} = 0.40 cm^3/g. (c) Schematic of the mechanism involved in hierarchal pore formation. The picture is consistent with the enthalpy changes of solvent crystals.

Figure 12 shows that DMAc-10 has an anisotropic macroporous morphology in which the macropores on the air side are significantly larger than those on the glass side. The skeleton has a fishbone-like morphology in the thickness direction that originates from the directional crystal growth of solvent macrocrystals, similar to that observed in previous studies.[35,36] Solvent crystals therefore nucleate at the sample layer of the glass side and, due to the temperature gradient, grow toward the air side. Mesopores were observed on the walls of the framework and the hierarchal

pores have a large S_{BET} of 97 m^2/g and a V_{meso} of 0.18 cm^3/g (Figure S6), which is different to previously reported systems.

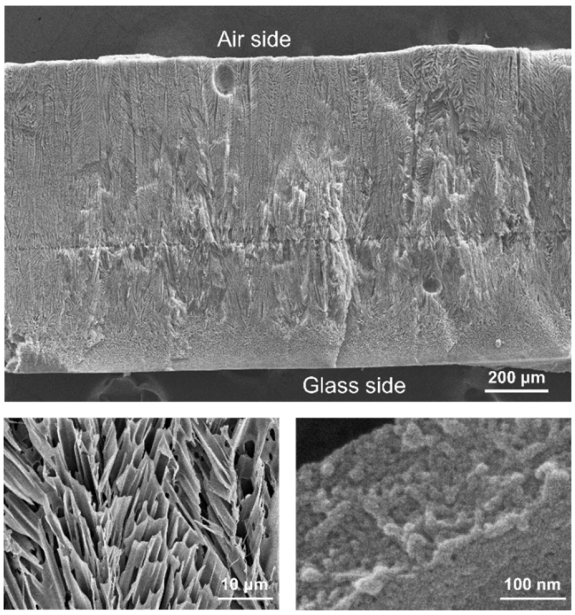

Figure 12. Cross-sectional SEM images of the DMAc-10 porous polystyrene.

Bimodal mesopores

The use of a solvent with a moderate T_b/T_m ratio occasionally resulted in bimodally distributed mesopores, as evidenced by N_2-adsorption studies and referred to as "bimodal mesopores." For example, DCB (T_b/T_m = 1.77) produced DCB-30, which exhibits a bimodal pore-size distribution with peaks at 25 and 11 nm (Figure 13(a)); these bimodal mesopores were also imaged by SEM (Figure 13(b)). Similarly, NB (T_b/T_m = 1.74) gave NB-35, which exhibits bimodal mesopores with d_{peak} values of 33 and 11 nm, and NB-30 with bimodal mesopores at d_{peak} values of 37 and 12 nm (Figure 13(c)); these results are consistent with the SEM image in Figure 13(d). The bimodal mesopores are evidently different from the uniform mesopore distribution observed for

NB-40 as well as the macropores of NB-20. The mechanism for the formation of bimodal mesopores suggests that nanocrystallization is initiated twice with a delayed interval, as schematically illustrated in Figure 13(e). Initially, a small number of crystal nuclei appear sparsely due to the moderate T_b/T_m ratio; they then grow slowly in the highly viscous solution. Further crystal nuclei are generated in the concentrated solution phase in a delayed manner prior to complete growth of the initial crystal nuclei, which rapidly terminates their crystal growth due to the high C_{PS} value. Large and small solvent nanocrystals are obtained from the initial and second sets of nuclei, respectively, at the end of the crystal-growth process. The presence of two sets of solvent nanocrystals with different sizes finally leads to a bimodal mesopore distribution.

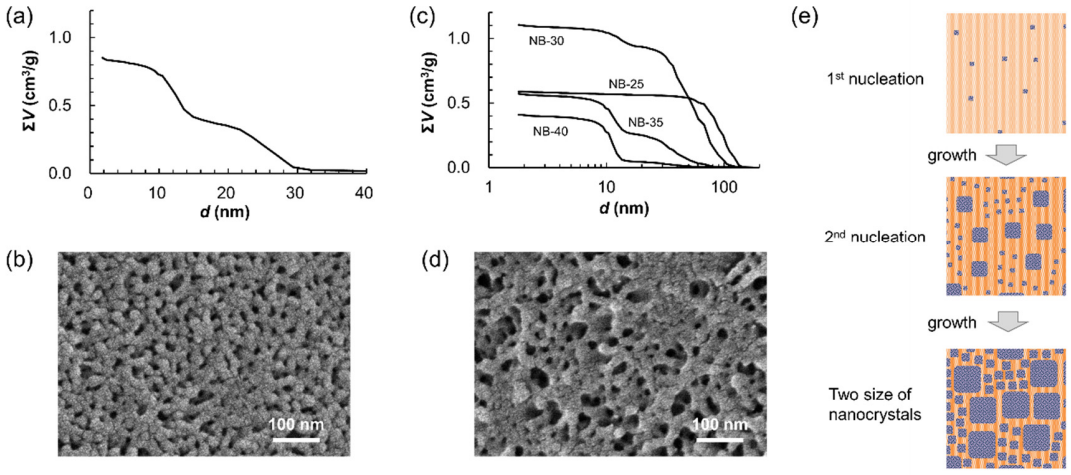

Figure 13. Bimodal mesopores of DCB-30: (a) cumulative pore volume and (b) cross-sectional SEM image. (c) Pore-size distributions of NB-25, -30, -35, -40, and (d) cross-sectional SEM image of NB-30. (e) Schematic illustration of the two-step crystal-nucleation of solvent molecules at low temperature. The second nucleation occurs in the concentrated polymer solution phase between the initially nucleated crystals. Larger nanocrystals form from earlier nucleation, while smaller nanocrystals form from later nucleation.

A porous polystyrene morphology diagram is shown in Figure 14(a) based on the C_{PS} values and the T_b/T_m ratios of the solvents, the discussion presented above, and the results summarized in Table S1. Notably, the data for the CCl system deviates from the overall trend of the other solvents due to the significantly higher CCl density. The four types of porous morphology are mainly located in the isolated regions of the diagram. More specifically, the macroporous morphology appeared at low T_b/T_m, hierarchal pores were formed at low C_{PS} using solvents with high T_b/T_m ratios, uniform mesopores were obtained at both high C_{PS} and high T_b/T_m, and bimodal mesopores occasionally appeared at moderate C_{PS} values and T_b/T_m ratios. Consequently, our flash freezing method produces a variety of pore morphologies through judicious choice of the C_{PS} value and T_b/T_m ratio, as schematically illustrated in Figure 14(b).

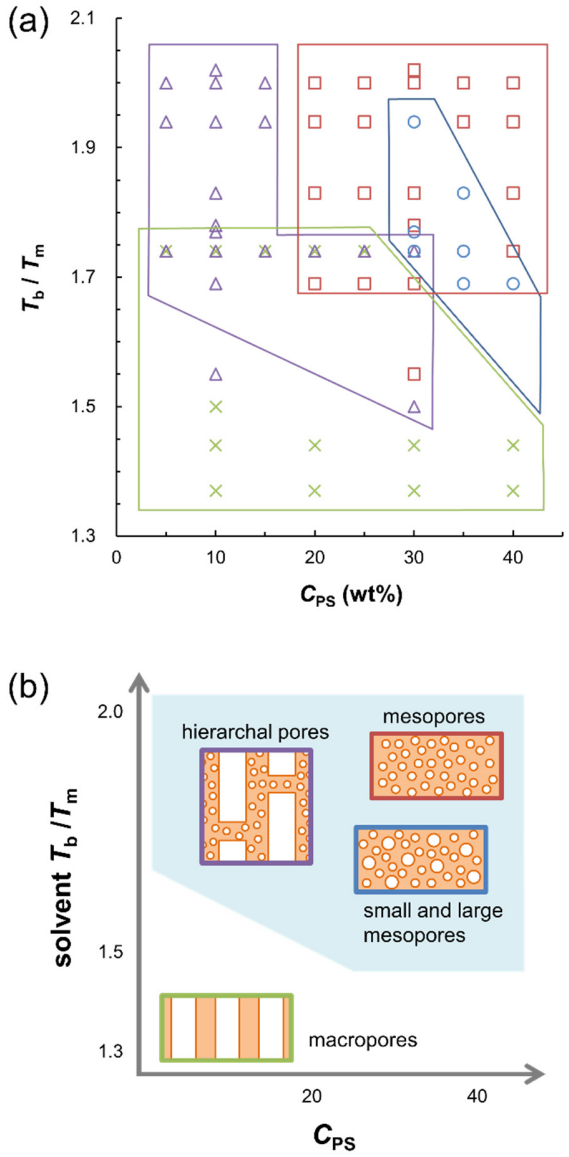

Figure 14. (a) Morphology diagram for porous polystyrenes with respect to the C_{PS} value and the T_b/T_m ratio of the solvent. The four types of porous structure are represented by different symbols: crosses = macropores, triangles = hierarchal pores, circles = bimodal pores, and squares = uniform mesopores. (b) Schematic representation of the morphology diagram.

CONCLUSION

We demonstrated that the flash freezing method can be used to fabricate mesoporous polystyrenes in a template-free manner. The solvent effect was comprehensively investigated using 13 good solvents for polystyrene, and the effect of C_{PS} was also evaluated. The crystallization behavior of each solution was explained on the basis of the obtained phase diagram and crystallization kinetics. Three key factors were found to be responsible for generating mesoporous polystyrenes with narrow pore-size distributions: (1) flash freezing, (2) a high C_{PS}, and (3) a solvent with low kinetic crystallizability, which correlate well with a high solvent T_b/T_m ratio, as previously suggested by research into glassy materials. These factors prevent unintentional crystallization during flash freezing to a low crystallization temperature and enable the solvent to crystallize at a low temperature, ultimately leading to the formation of mesopores. In contrast, solvents with low T_b/T_m values only generate macropores, with morphologies similar to those produced by the previously reported ice templating and solvent casting methods. A low C_{PS} frequently led to hierarchical structures composed of mesopores and macropores, while moderate C_{PS} and T_b/T_m values occasionally formed bimodal mesopores. The abovementioned three factors distinguish this method from conventional ice templating and freeze casting methods. Therefore, the selection of a good solvent in addition to an optimal polymer concentration can lead to desirable porous structures with sophisticated designs, aided by a morphology diagram based on the solvent T_b/T_m ratio and the C_{PS} value. The obtained results enable the processing parameters required to produce hierarchal pores to be extended using a solvent mixture with either low or high T_b/T_m value. Hierarchal pores can also be fabricated using the flash freezing method by implementing other well-established methods for macropore design. We expect that the flash freezing method developed in this study will also be applicable to polymer solutions retained in porous media, such as nonwoven sheets and

macroporous sponges, which will ultimately lead to the production of mechanically-strong mesoporous composites. The developed method is expected to provide nanoparticle-functionalized mesoporous polymers using polymer solutions of metal, carbon, or inorganic nanoparticles; such polymers are promising materials for energy, environmental, and biomedical applications. We are currently exploring novel applications of the flash freezing method and will report the results in due course.

ASSOCIATED CONTENT

Supporting Information: SEM images and pore-size distributions of mesoporous polystyrenes, data for Diox and pXy solutions, numerical calculation of mesopore size, DSC profiles of 10-wt% polystyrene solutions following flash freezing, tabulated pore properties of porous polystyrenes prepared in this study.

AUTHOR INFORMATION

Corresponding Author

*To whom correspondence should be addressed: SAMITSU.Sadaki@nims.go.jp

Present Addresses

†Institute of Materials Research and Engineering, Agency for Science, Technology and Research (A*STAR), 2 Fusionopolis Way, 138634 Singapore

Author Contributions

S.S. and I.I conceived the concept of flash freezing. S.S. conducted the experiments, analyzed the data. S.P. and H.Y supported the SAXS. S.S. and I.I. wrote the manuscript. All authors have given approval to the final version of the manuscript.

ACKNOWLEDGMENT

The authors are grateful to Prof. Masanobu Naito of NIMS for instrumental support. SAXS was performed with the approval of the Photon Factory Program Advisory Committee (Proposal No. 2018G019). S.S. acknowledges financial support provided by JSPS KAKENHI Grants JP26410230, JP17K06007, and 21H02006. S.P. acknowledges a NIMS Junior Researcher Research Fellowship (2017–2018).

REFERENCES

(1) Notario, B.; Pinto, J.; Rodriguez-Perez, M. A. Nanoporous Polymeric Materials: A New Class of Materials with Enhanced Properties. *Prog. Mater. Sci.* **2016**, *78–79*, 93–139, DOI 10.1016/j.pmatsci.2016.02.002.

(2) Wu, D.; Xu, F.; Sun, B.; Fu, R.; He, H.; Matyjaszewski, K. Design and Preparation of Porous Polymers. *Chem. Rev.* **2012**, *112* (7), 3959–4015, DOI 10.1021/cr200440z.

(3) Jackson, E. A.; Hillmyer, M. A. Nanoporous Membranes Derived from Block Copolymers: From Drug Delivery to Water Filtration. *ACS Nano* **2010**, *4* (7), 3548–3553, DOI 10.1021/nn1014006.

(4) Deng, H.; Grunder, S.; Cordova, K. E.; Valente, C.; Furukawa, H.; Hmadeh, M.; Gandara, F.; Whalley, A. C.; Liu, Z.; Asahina, S.; Kazumori, H.; O'Keeffe, M.; Terasaki, O.; Stoddart, J. F.; Yaghi, O. M. Large-Pore Apertures in a Series of Metal-Organic Frameworks. *Science* **2012**, *336* (6084), 1018–1023, DOI 10.1126/science.1220131.

(5) Yue, Y.; Mayes, R. T.; Kim, J.; Fulvio, P. F.; Sun, X.-G.; Tsouris, C.; Chen, J.; Brown, S.; Dai, S. Seawater Uranium Sorbents: Preparation from a Mesoporous Copolymer Initiator by Atom-Transfer Radical Polymerization. *Angew. Chem. Int. Ed.* **2013**, *52* (50), 13458–13462, DOI 10.1002/anie.201307825.

(6) Zhou, W.; Gao, H.; Goodenough, J. B. Low-Cost Hollow Mesoporous Polymer Spheres and All-Solid-State Lithium, Sodium Batteries. *Adv. Energy Mater.* **2016**, *6* (1), 1501802, DOI 10.1002/aenm.201501802.

(7) Johnson, S. A.; Ollivier, P. J.; Mallouk, T. E. Ordered Mesoporous Polymers of Tunable Pore Size from Colloidal Silica Templates. *Science* **1999**, *283* (5404), 963–965, DOI 10.1126/science.283.5404.963.

(8) Uehara, H.; Tamura, T.; Kakiage, M.; Yamanobe, T. Nanowrinkled and Nanoporous Polyethylene Membranes via Entanglement Arrangement Control. *Adv. Funct. Mater.* **2012**, *22* (10), 2048–2057, DOI 10.1002/adfm.201102474.

(9) Forest, C.; Chaumont, P.; Cassagnau, P.; Swoboda, B.; Sonntag, P. Polymer Nano-Foams for Insulating Applications Prepared from CO2 Foaming. *Prog. Polym. Sci.* **2015**, *41* (C), 122–145, DOI 10.1016/j.progpolymsci.2014.07.001.

(10) Samitsu, S. Thermally Stable Mesoporous Poly(Ether Sulfone) Monoliths with Nanofiber Network Structures. *Macromolecules* **2018**, *51* (1), 151–160, DOI 10.1021/acs.macromol.7b02217.

(11) Li, L.; Yokoyama, H.; Nemoto, T.; Sugiyama, K. Facile Fabrication of Nanocellular Block Copolymer Thin Films Using Supercritical Carbon Dioxide. *Adv. Mater.* **2004**, *16* (14), 1226–1229, DOI 10.1002/adma.200400264.

(12) Zhou, N.; Bates, F. S.; Lodge, T. P. Mesoporous Membrane Templated by a Polymeric Bicontinuous Microemulsion. *Nano Lett.* **2006**, *6* (10), 2354–2357, DOI 10.1021/nl061765t.

(13) Uehara, H.; Yoshida, T.; Kakiage, M.; Yamanobe, T.; Komoto, T.; Nomura, K.; Nakajima, K.; Matsuda, M. Nanoporous Polyethylene Film Prepared from Bicontinuous Crystalline/Amorphous Structure of Block Copolymer Precursor. *Macromolecules* **2006**, *39* (12), 3971–3974, DOI 10.1021/ma0601316.

(14) Zalusky, A. S.; Olayo-Valles, R.; Wolf, J. H.; Hillmyer, M. A. Ordered Nanoporous Polymers from Polystyrene-Polylactide Block Copolymers. *J. Am. Chem. Soc.* **2002**, *124* (43), 12761–12773, DOI 10.1021/ja0278584.

(15) Li, L.; Yokoyama, H.; Nemoto, T.; Sugiyama, K. Facile Fabrication of Nanocellular Block Copolymer Thin Films Using Supercritical Carbon Dioxide. *Adv. Mater.* **2004**, *16* (14), 1226–1229, DOI 10.1002/adma.200400264.

(16) Meng, Y.; Gu, D.; Zhang, F.; Shi, Y.; Yang, H.; Li, Z.; Yu, C.; Tu, B.; Zhao, D. Ordered Mesoporous Polymers and Homologous Carbon Frameworks: Amphiphilic Surfactant

Templating and Direct Transformation. *Angew. Chem. Int. Ed.* **2005**, *44* (43), 7053–7059, DOI 10.1002/anie.200501561.

(17) Park, S.; Wang, J. Y.; Kim, B.; Xu, J.; Russell, T. P. A Simple Route to Highly Oriented and Ordered Nanoporous Block Copolymer Templates. *ACS Nano* **2008**, *2* (4), 766–772, DOI 10.1021/nn7004415.

(18) Hirai, T.; Leolukman, M.; Liu, C. C.; Han, E.; Kim, Y. J.; Ishida, Y.; Hayakawa, T.; Kakimoto, M. A.; Nealey, P. F.; Gopalan, P. One-Step Direct-Patterning Template Utilizing Self-Assembly of POSS-Containing Block Copolymers. *Adv. Mater.* **2009**, *21* (43), 4334–4338, DOI 10.1002/adma.200900518.

(19) Olson, D. A.; Chen, L.; Hillmyer, M. A. Templating Nanoporous Polymers with Ordered Block Copolymers. *Chem. Mater.* **2008**, *20* (3), 869–890, DOI 10.1021/cm702239k.

(20) Dorin, R. M.; Sai, H.; Wiesner, U. Hierarchically Porous Materials from Block Copolymers. *Chem. Mater.* **2014**, *26* (1), 339–347, DOI 10.1021/cm4024056.

(21) Sai, H.; Tan, K. W.; Hur, K.; Asenath-Smith, E.; Hovden, R.; Jiang, Y.; Riccio, M.; Muller, D. A.; Elser, V.; Estroff, L. A.; Gruner, S. M.; Wiesner, U. Hierarchical Porous Polymer Scaffolds from Block Copolymers. *Science* **2013**, *341*, 530–534, DOI 10.1126/science.1238159.

(22) Tan, K. W.; Jung, B.; Werner, J. G.; Rhoades, E. R.; Thompson, M. O.; Wiesner, U. Transient Laser Heating Induced Hierarchical Porous Structures from Block Copolymer–Directed Self-Assembly. *Science* **2015**, *349*, 54–58, DOI 10.1126/science.aab0492.

(23) Cheng, S. Z. D. *Phase Transitions in Polymers*; Elsevier, 2008, DOI 10.1016/B978-0-444-51911-5.X0001-1.

(24) van de Witte, P.; Dijkstra, P. J. J.; van den Berg, J. W. a. W. a; Feijen, J. Phase Separation Processes in Polymer Solutions in Relation to Membrane Formation. *J. Membr. Sci.* **1996**, *117* (1–2), 1–31, DOI 10.1016/0376-7388(96)00088-9.

(25) Strobl, G. R. *The Physics of Polymers*; Springer, 2007, DOI 10.1007/978-3-540-68411-4.

(26) Mulder, M. *Basic Principles of Membrane Technology*; Springer, 1996, DOI 10.1007/978-94-009-1766-8.

(27) Lloyd, D. R.; Kim, S. S.; Kinzer, K. E. Microporous Membrane Formation via Thermally-Induced Phase Separation. II. Liquid-Liquid Phase Separation. *J. Membr. Sci.* **1991**, *64* (1–2), 1–11, DOI 10.1016/0376-7388(91)80073-F.

(28) Song, S. W.; Torkelson, J. M. Coarsening Effects on Microstructure Formation in Isopycnic Polymer Solutions and Membranes Produced via Thermally Induced Phase Separation. *Macromolecules* **1994**, *27* (22), 6389–6397, DOI 10.1021/ma00100a024.

(29) Aubert, J. H. Structural Coarsening of Demixed Polymer Solutions. *Macromolecules* **1990**, *23* (5), 1446–1452, DOI 10.1021/ma00207a034.

(30) Mandelkern, L. *Crystallization of Polymers*, Second Ed.; Cambridge University Press: New York, 2002, DOI 10.1017/CBO9780511541315.

(31) Lloyd, D. R.; Kinzer, K. E.; Tseng, H. S. Microporous Membrane Formation via Thermally Induced Phase Separation. I. Solid-Liquid Phase Separation. *J. Membr. Sci.* **1990**, *52* (3), 239–261, DOI 10.1016/S0376-7388(00)85130-3.

(32) Gutiérrez, M. C.; Ferrer, M. L.; Del Monte, F. Ice-Templated Materials: Sophisticated Structures Exhibiting Enhanced Functionalities Obtained after Unidirectional Freezing and Ice-Segregation- Induced Self-Assembly. *Chem. Mater.* **2008**, *20* (3), 634–648, DOI 10.1021/cm702028z.

(33) Deville, S.; Saiz, E.; Nalla, R. K.; Tomsia, A. P. Freezing as a Path to Build Complex Composites. *Science* **2006**, *311*, 515–518, DOI 10.1126/science.1120937.

(34) Li, W. L.; Lu, K.; Walz, J. Y. Freeze Casting of Porous Materials: Review of Critical Factors in Microstructure Evolution. *Int. Mater. Rev.* **2012**, *57* (1), 37–60, DOI 10.1179/1743280411Y.0000000011.

(35) Zhang, H.; Hussain, I.; Brust, M.; Butler, M. F.; Rannard, S. P.; Cooper, A. I. Aligned Two- and Three-Dimensional Structures by Directional Freezing of Polymers and Nanoparticles. *Nat. Mater.* **2005**, *4* (10), 787–793, DOI 10.1038/nmat1487.

(36) Wang, B.; Ji, J.; Li, K. Crystal Nuclei Templated Nanostructured Membranes Prepared by Solvent Crystallization and Polymer Migration. *Nat. Commun.* **2016**, *7*, 12804, DOI 10.1038/ncomms12804.

(37) Gutiérrez, M. C.; García-Carvajal, Z. Y.; Jobbágy, M.; Rubio, F.; Yuste, L.; Rojo, F.; Ferrer, M. L.; Del Monte, F. Poly(Vinyl Alcohol) Scaffolds with Tailored Morphologies for Drug Delivery and Controlled Release. *Adv. Funct. Mater.* **2007**, *17* (17), 3505–3513, DOI 10.1002/adfm.200700093.

(38) Papon, P.; Leblond, J.; Meijer, P. H. E. *The Physics of Phase Transitions*; Springer, 2006, DOI 10.1007/3-540-33390-8.

(39) Samitsu, S.; Zhang, R.; Peng, X.; Krishnan, M. R.; Fujii, Y.; Ichinose, I. Flash Freezing Route to Mesoporous Polymer Nanofibre Networks. *Nat. Commun.* **2013**, *4* (1), 2653, DOI 10.1038/ncomms3653.

(40) Krishnan, M. R.; Samitsu, S.; Fujii, Y.; Ichinose, I. Hydrophilic Polymer Nanofibre Networks for Rapid Removal of Aromatic Compounds from Water. *Chem. Commun.* **2014**, *50* (66), 9393–9396, DOI 10.1039/C4CC01786B.

(41) Marcus, Y. *The Properties of Solvents*; Wiley, 1998.

(42) Linstrom P. J.; Mallard, W. G. Chemistry WebBook, NIST Standard Reference Database Number 69 http://webbook.nist.gov. Accessed 8 February 2017, DOI 10.18434/T4D303.

(43) Takagi, H.; Igarashi, N.; Mori, T.; Saijo, S.; Ohta, H.; Nagatani, Y.; Kosuge, T.; Shimizu, N. Upgrade of Small Angle X-Ray Scattering Beamline BL-6A at the Photon Factory. *AIP Conf. Proc.* **2016**, *1741*, 30018, DOI 10.1063/1.4952841.

(44) Shimizu, N.; Yatabe, K.; Nagatani, Y.; Saijyo, S.; Kosuge, T.; Igarashi, N. Software Development for Analysis of Small-Angle X-Ray Scattering Data. *AIP Conf. Proc.* **2016**, *1741*, 50017, DOI 10.1063/1.4952937.

(45) Klein, M.; Guenet, J. M. Effect of Polymer Chain Microstructure on Solvent Crystallization: Implications on Polymer Solvation and on Physical Gelation. *Macromolecules* **1989**, *22* (9), 3716–3725, DOI 10.1021/ma00199a036.

(46) Kalogeras, I. M.; Brostow, W. Glass Transition Temperatures in Binary Polymer Blends. *J. Polym. Sci. Part B: Polym. Phys.* **2009**, *47*, 80–95, DOI 10.1002/polb.

(47) Angell, C. A.; Sare, J. M.; Sare, E. J. Glass Transition Temperatures for Simple Molecular Liquids and Their Binary Solutions. *J. Phys. Chem.* **1978**, *82* (24), 2622–2629, DOI 10.1021/j100513a016.

(48) Turnbull, D.; Cohen, M. H. Concerning Reconstructive Transformation and Formation of Glass. *J. Chem. Phys.* **1958**, *29* (5), 1049–1054, DOI 10.1063/1.1744654.

(49) Hou, Q.; Grijpma, D. W.; Feijen, J. Preparation of Interconnected Highly Porous Polymeric Structures by a Replication and Freeze-Drying Process. *J. Biomed. Mater. Res., Part B* **2003**, *67* (2), 732–740, DOI 10.1002/jbm.b.10066.

(50) Nail, S. L.; Jiang, S.; Chongprasert, S.; Knopp, S. A. Fundamentals of Freeze-Drying. In *Development and Manufacture of Protein Pharmaceuticals. Pharmaceutical Biotechnology, vol 14.*; Springer, 2002; pp 281–360, DOI 10.1007/978-1-4615-0549-5_6.

(51) de Groot, J. H.; Nijenhuis, A. J.; Bruin, P.; Pennings, A. J.; Veth, R. P. H.; Klompmaker, J.; Jansen, H. W. B. Use of Porous Biodegradable Polymer Implants in Meniscus Reconstruction. 1) Preparation of Porous Biodegradable Polyurethanes for the Reconstruction of Meniscus Lesions. *Colloid Polym. Sci.* **1990**, *268* (12), 1073–1081, DOI 10.1007/BF01410672.

(52) Huang, P.-T.; Chang, Y.-S.; Chou, C.-W. Preparation of Porous Poly(3-Hexylthiophene) by Freeze-Dry Method and Its Application to Organic Photovoltaics. *J. Appl. Polym. Sci.* **2011**, *122* (1), 233–240, DOI 10.1002/app.34132.

(53) Mandelkern, L. *Crystallization of Polymers Volume 2: Kinetics and Mechanisms*; Cambridge University Press, 2004, DOI 10.1017/CBO9780511535413.